Chinese Journal of Natural Medicines

Novel araucarene diterpenes from *Agathis dammara* exert hypoglycemic activity by promoting pancreatic β cell regeneration and glucose uptake

Zhewei Yu, Yi Zhang, Wenhui Wang, XinYi Wu, Shunzhi Liu, Yanlin Bin, Hongsheng Li, Bangping Cai, Zheng Wang, Meijuan Fang, Rong Qi, Mingyu Li, Yingkun Qiu

Citation: Zhewei Yu, Yi Zhang, Wenhui Wang, XinYi Wu, Shunzhi Liu, Yanlin Bin, Hongsheng Li, Bangping Cai, Zheng Wang, Meijuan Fang, Rong Qi, Mingyu Li, Yingkun Qiu, Novel araucarene diterpenes from *Agathis dammara* exert hypoglycemic activity by promoting pancreatic β cell regeneration and glucose uptake, Chinese Journal of Natural Medicines, 2025, 23(4), 492−503. doi: 10.1016/S1875−5364(25)60856−9.

View online: https://doi.org/10.1016/S1875−5364(25)60856−9

Chinese Journal of Natural Medicines 23 (2025) 492-503

Contents lists available at ScienceDirect

Chinese Journal of Natural Medicines

journal homepage: www.cjnmcpu.com/

Original article

Novel araucarene diterpenes from *Agathis dammara* exert hypoglycemic activity by promoting pancreatic β cell regeneration and glucose uptake

Zhewei Yu[a,b,Δ], Yi Zhang[a,Δ], Wenhui Wang[a], XinYi Wu[a], Shunzhi Liu[a], Yanlin Bin[a], Hongsheng Li[a], Bangping Cai[c], Zheng Wang[d], Meijuan Fang[a], Rong Qi[b], Mingyu Li[a,*], Yingkun Qiu[a,*]

[a] *School of Pharmaceutical Sciences, Xiamen University, Xiamen 361102, China*
[b] *School of Basic Medical Sciences, Peking University, Beijing 100191, China*
[c] *Xiamen Botanical Garden, Xiamen 361003, China*
[d] *Zhongshan Hospital Affiliated to Xiamen University, Xiamen 361001, China*

ARTICLE INFO

Article history:
Received 23 January 2024
Revised 19 April 2024
Accepted 7 May 2024
Available online 20 April 2025

Keywords:
Agathis dammara
Araucarene
Diterpenes
Hypoglycemic
Pancreatic β Cells

ABSTRACT

In this study, araucarene diterpenes, characterized by a pimarene skeleton with a variably oxidized side chain at C-13, were investigated. A total of 16 araucarene diterpenoids and their derivatives were isolated from the woods of *Agathis dammara*, including 11 previously unreported compounds: dammaradione (**1**), dammarones D–G (**2**, **5**, **14**, **15**), dammaric acids B–F (**8**–**12**), and dammarol (**16**). The structures of these new compounds were elucidated using high-resolution electrospray ionization mass spectroscopy (HR-ESI-MS) and one-dimensional/two-dimensional (1D/2D) nuclear magnetic resonance (NMR), while their absolute configurations were determined through the electronic circular dichroism (ECD) exciton chirality method and Snatzke's method. The hypoglycemic activity of all isolated compounds was evaluated using a transgenic zebrafish model, and a structure–activity relationship (SAR) analysis was conducted. Araucarone (**3**) and dammaric acid C (**9**), serving as representative compounds, demonstrated significant hypoglycemic effects on zebrafish. The primary mechanism involves the promotion of pancreatic β cell regeneration and glucose uptake. Specifically, these compounds enhance the differentiation of pancreatic endocrine precursor cells (PEP cells) into β cells in zebrafish.

1. Introduction

The hypoglycemic effect is a vital biological activity exhibited by numerous natural-origin compounds, conferring significant medicinal value in addressing various health conditions, including cardiovascular diseases, diabetes, metabolic syndrome, and obesity [1-4]. Araucariaceae, an ancient family of tall trees, is predominantly found in the southern hemisphere, while *Agathis dammara* is a species located in Malaysia in the northern hemisphere [5]. Araucarene, encompassing a series of diterpene compounds extracted from Araucariaceae family plants, has been historically underappreciated, with limited research focusing on its basic chemical structure dating back to the 1960s [6, 7]. Notably, the wood resin of *A. dammara*, known as dammara resin, finds extensive applications in industry and medicine [8]. Malaysian indigenous populations have traditionally employed it to address various inflammatory-related conditions, including arthritis, headaches, muscle pain, burns, fever, diarrhea, and abdominal discomfort [9]. Compounds isolated from this resin are also believed to possess potential biological activities, such as hypoglycemic, hypolipidemic, antioxidant, and anti-inflammatory effects [8]. In a parallel investigation, we discovered that the total diterpene content of *A. dammara* and one monomeric araucarene diterpene derived from it effectively inhibited the progression of abdominal aortic aneurysm by suppressing the activation of the NF-κB/NLRP3 pathway [10]. Understanding the active derivatives of araucarene diterpenes and their pharmacological effects in *A. dammara* wood extract, as well as the specific mechanisms involved, is essential for harnessing the potential of this plant as a natural therapeutic agent.

This study reports the isolation of 16 araucarene diterpenoids and their derivatives from the wood extract of *A. dammara*, with 11 of these compounds being novel discoveries. The structures of the new compounds were elucidated using high-resolution electrospray ionization mass spectroscopy (HR-ESI-MS) and one-dimensional/two-dimensional (1D/2D) nuclear magnetic resonance (NMR), while their absolute configurations were determined through electronic circular dichroism (ECD) exciton chirality method and Snatzke's method. These novel compounds were designated as dammaradione (**1**), dammarones D–G (**2**, **5**, **14**, **15**), dammaric acids B–F (**8**–**12**), and dammarol (**16**). The hypoglycemic activity of these diterpenoids was subsequently evaluated using zebrafish models, and a structure-activity relationship analysis was conducted. Furthermore, the

* Corresponding author.
E-mail addresses: limingyu@xmu.edu.cn (M. Li); qyk@xmu.edu.cn (Y. Qiu)
Δ These authors contributed equally to this work.

https://doi.org/10.1016/S1875-5364(25)60856-9

biological mechanism underlying their hypoglycemic action was investigated. The findings indicate that the active compounds promote pancreatic β cell regeneration by stimulating the differentiation of zebrafish pancreatic endocrine precursor cells (PEP cells) into β cells. Additionally, these compounds were observed to enhance glucose uptake in zebrafish. This paper presents the isolation, structural identification, hypoglycemic biological evaluation, and mechanistic studies of these compounds.

2. Results and Discussion

2.1. Separation and structural identification of compounds

The 16 araucarene diterpenes and their derivatives isolated in this study (Fig. 1) were all observed as white powders. The ^{13}C NMR spectral data (Table 1) exhibited a high degree of similarity in internal structure, with only minor differences attributable to varying substituents on specific carbon atoms. These variations served as a crucial basis for determining the structure of the novel compounds identified in this investigation . ^{1}H NMR spectral data (Table 2) and 2D NMR techniques, including heteronuclear singular quantum correlation (HSQC), heteronuclear multiple bond correlation (HMBC), and correlation spectroscopy (COSY), were employed to elucidate the planar configuration of the new compounds (Fig. 2), while nuclear Overhauser effect spectroscopy (NOESY) signals were utilized to confirm their relative configuration (Fig. 3). Additionally, the determination of HR-ESI-MS, ultraviolet (UV) spectrum, infrared (IR) spectrum, and optical rotation provided further significant insights into the structure of the novel compounds. The absolute configuration of these new compounds was established by comparing the measured and calculated values of their ECD spectra (Fig. 4).

Dammaradione (**1**), a white powder, exhibited a molecular formula of $C_{20}H_{30}O_2$, indicating 6 degrees of unsaturation, as determined by HR-ESI-MS at a mass-to-charge ratio (*m/z*) 303.2317 $[M + H]^+$ (Calcd. for $C_{20}H_{31}O_2$, 303.2319). In ^{1}H NMR spectrum (Table 2) revealed four typical methyl signals at δ_H 1.04 (3H, s, H-17), 1.14 (3H, s, H-18), 1.08 (3H, s, H-19), 1.09 (3H, s, H-20), consistent with an araucarone diterpenoid structure. Additionally, an atypical methyl signal appeared at δ_H 2.15 (3H, s, H-16). An alkene hydrogen signal was observed at δ_H 5.48 (1H, m, H-7), corresponding to an in-ring double bond, as evidenced by the ^{13}C NMR (Table 1) signals at δ_C 122.5 (C-7) and 134.3 (C-8). The DEPT spectrum indicated the presence of five primary carbons, six secondary carbons, three tertiary carbons, and five quaternary carbons, including two carbonyl groups at δ_C 216.8 (C-3) and 214.0 (C-15) in the ^{13}C NMR spectrum. The planar structure of the molecule was elucidated through analysis of HSQC, COSY, and HMBC spectra (Fig. 2). Key HMBCs demonstrated the connection from δ_H 2.15 (s, CH_3-16) to δ_C 214.0 (C-15), from δ_H 1.04 (s, CH_3-17) to δ_C 47.8 (C-13) and then to δ_C 32.5 (C-12), 41.8 (C-14), 214.0 (C-15), from δ_H 1.14 (s, CH_3-18) and 1.08 (s, CH_3-19) to δ_C 47.4 (C-4) and then to δ_C 216.8 (C-3) and 51.5 (C-5), and from δ_H 1.09 (s, CH_3-20) to δ_C 47.8 (C-10) and then to δ_C 38.0 (C-1), 51.5 (C-5), 50.7 (C-9). The structure of **1** resembles that of the known compound araucarone (**3**), with the notable difference being the absence of the 16-hydroxyl group, resulting in C-16 becoming a methyl group (δ_C 24.8). These NMR data confirmed the planar structure of **1**.

The specific optical rotation of **1** is $[\alpha]_D^{25}$ −10 (*c* 0.1 MeOH). The NOESY signals between δ_H 1.09 (s, CH_3-20), 1.43 (m, β-H-4), 1.04 (s, CH_3-17), and 1.14 (s, CH_3-18), as well as the correlations between 1.14 (s, CH_3-19), 1.58 (m, H-5), and 1.71 (m, H-9), indicated that CH_3-20, CH_3-17, CH_3-18 exhibit β configurations, while H-5, H-9, CH_3-19 demonstrate α configuration (Fig. 3). To determine its absolute configuration, quantum mechanical calculations of the ECD spectrum of **1** were conducted using the time-dependent density functional theory method. The calculated ECD spectrum, obtained at the B3LYP/6-31G + (d) level, aligned precisely with the experimental results (Fig. 4), suggesting the absolute configuration of the compound is 5*R*, 9*S*, 10*R*, 13*S*.

Dammarone D (**2**) was obtained as a white powder with NMR signals similar to those of **3** (Table 1). Its molecular formula, $C_{20}H_{32}O_3$, was determined by an ion peak in HR-ESI-MS at *m/z* 321.2422 $[M + H]^+$ (Calcd. for $C_{20}H_{33}O_3$, 321.2424), indicating 5 degrees of unsaturation. The primary difference between **2** and **3** is in the A ring. Hydroxyl signals were observed in ^{1}H NMR and ^{13}C NMR at δ_H 3.47 (1H, t, H-3) and δ_C 76.0 (C-3), respectively. Furthermore, the NMR signals of **2** closely resemble those of the known compound araucarol (**7**), except for the signals of C-1–C-5 and C-18 on the A ring, attributable to hydroxyl isomerization at C-3 from β configuration (δ_C 79.1 of **7**) to α configuration (δ_C 76.0 of **2**). HMBS, HSQC, and COSY signals support the proposed planar structure (Fig. 2). The isomerization was confirmed by the correlation between δ_H 3.47 (t, H-3) and 0.95 (s, CH_3-18) in the NOESY (Fig. 3) and specific optical rotation $[\alpha]_D^{25}$ −24 (*c* 0.1 MeOH). Comparison of the Cotton effect observed in ECD with calculated values indicates that the configuration of **2** is 3*R*, 5*R*, 9*S*, 10*R*, 13*S* (Fig. 4).

Dammarone E (**5**) was isolated as a white powder with a specific optical rotation of $[\alpha]_D^{25}$ −22 (*c* 0.1, MeOH). Its molecular formula, $C_{20}H_{30}O_4$, requiring 6 degrees of unsaturation, was determined by HR-ESI-MS *m/z* 335.2215 $[M + H]^+$ (Calcd. for $C_{20}H_{31}O_4$, 335.2217). The NMR signals of **5** closely resemble those of **3**, with the primary difference observed at the C-2 position. The ^{13}C NMR signal for C-2 shifted from δ_C 34.6 of **3** to δ_C 68.7 of **5** (Table 1). The ^{1}H NMR signal at δ_H 4.57 (1H, m, H-2) confirms the presence of a hydroxyl substituent (Table 2). The planar structure was elucidated through analysis of various 2D NMR signals (Fig. 2). The

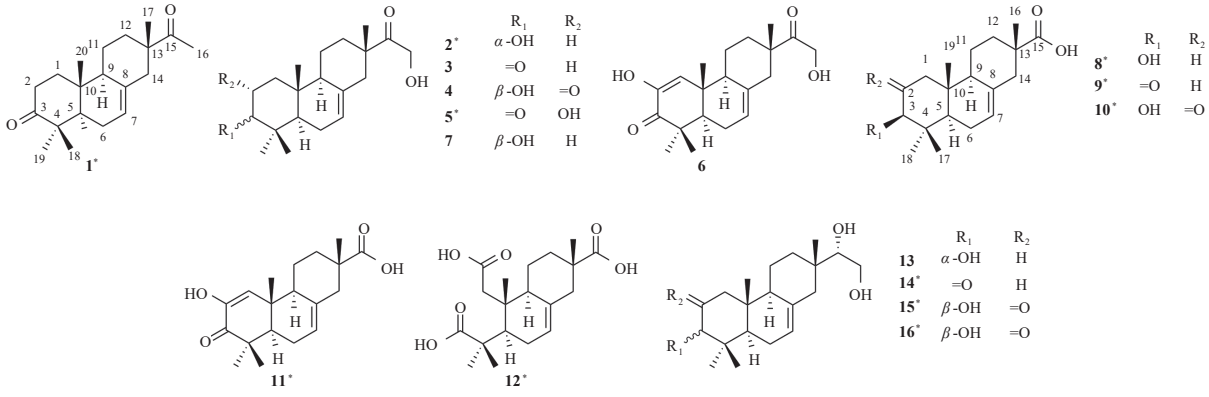

Fig. 1 Structure of araucarene diterpenoids and derivatives (**1**–**16**) isolated from *A. dammara* (*New compounds).

Table 1 ^{13}C NMR spectrum (150 MHz) data of isolated araucarene diterpenes and derivatives **1**–**16** (*New compounds).

Compd.	C-1	C-2	C-3	C-4	C-5	C-6	C-7	C-8	C-9	C-10	C-11	C-12	C-13	C-14	C-15	C-16	C-17	C-18	C-19	C-20
1*	38.0	34.6	216.8	47.4	51.5	23.8	122.5	134.3	50.7	35.2	19.8	32.5	47.8	41.8	214.0	24.8	19.2	22.6	25.5	14.8
2*	31.7	25.1	76.0	37.0	44.0	23.1	123.7	133.2	51.3	35.0	19.3	32.5	45.9	41.8	215.2	64.0	18.9	22.7	28.3	14.8
3	38.0	34.6	216.5	47.4	51.5	23.9	123.3	133.3	50.7	35.3	19.5	32.5	45.9	41.7	214.9	64.1	18.9	22.6	25.6	14.8
4	51.5	210.6	82.4	45.1	48.9	23.4	123.5	132.9	51.8	42.3	19.4	32.2	45.7	41.4	214.7	64.0	18.9	16.4	28.7	15.5
5*	47.9	68.7	216.0	47.0	52.3	23.7	122.8	133.1	50.8	35.8	19.3	32.3	45.8	41.5	214.7	64.0	18.9	22.6	25.0	15.6
6	123.6	143.7	200.5	43.4	48.1	22.9	123.8	133.1	48.6	36.4	19.3	32.4	45.9	42.0	214.7	64.1	19.0	22.5	25.4	16.0
7	37.8	27.3	79.1	38.6	49.8	23.2	123.5	133.0	51.5	35.4	18.9	32.6	45.9	41.7	215.2	64.0	19.3	15.7	28.4	14.9
8*	31.8	25.7	74.2	37.1	44.0	23.0	122.8	134.7	51.3	35.0	19.6	33.4	41.7	43.1	179.7	-	20.2	23.1	29.1	15.1
9*	38.0	34.6	216.8	47.5	51.6	23.8	122.7	133.9	50.6	35.2	19.6	33.0	42.1	42.4	183.9	-	19.7	22.6	25.6	14.8
10*	51.5	210.8	82.4	45.2	48.9	23.4	123.0	133.5	51.8	42.3	19.6	32.8	42.0	42.2	184.1	-	19.6	16.4	28.7	15.5
11*	124.0	143.7	200.7	43.5	48.1	22.8	123.2	133.7	48.6	36.4	19.5	32.9	42.2	42.7	184.4	-	19.8	22.5	25.4	16.0
12*	41.2	173.9	180.2	45.4	46.8	25.5	122.4	134.9	45.9	39.4	20.3	33.4	41.6	43.2	179.5	-	20.1	25.0	26.6	16.4
13	31.8	25.2	76.2	37.0	44.1	23.1	122.2	134.9	51.8	35.0	19.6	33.2	37.1	43.3	80.6	62.7	17.2	22.8	28.3	14.8
14*	38.2	34.7	217.2	47.5	51.2	23.9	121.7	135.0	51.7	35.3	19.8	33.0	37.1	43.0	80.4	62.7	17.3	22.7	25.6	14.8
15*	51.6	211.0	82.4	37.0	49.0	23.4	122.0	134.6	52.4	42.4	19.8	32.8	45.2	42.7	80.3	62.6	17.2	16.4	28.7	15.5
16*	37.9	27.7	77.5	38.7	50.1	23.2	121.3	136.0	52.1	35.3	19.9	33.3	37.4	43.4	80.0	62.5	17.6	16.5	29.0	15.2

[#]$CDCl_3$: **1**–**7**, **9**–**11**, **13**–**15**; DMSO-d_6: **8**, **12**, **16**.

NOESY correlation between δ_H 4.57 (m, H-2) and 1.19 (s, CH_3-20) indicated that the 2-hydroxyl group adopts an α configuration (Fig. 3). Comparison of ECD spectra further confirms the absolute configuration of **5** is 2*R*, 5*R*, 9*S*, 10*R*, 13*S* (Fig. 4).

Compounds **8**–**12** are 19-carbon diterpenes with a carboxyl group (C-15) at C-13. These compounds, rarely reported in literature, are designated as dammaric acids in this study. The formation of the carbonyl group and the absence of C-16 likely result from oxidative cleavage occurring between C-15 and C-16 (Fig. 2). To facilitate spectral data comparison (Tables 1 and 2), the carbon atom numbering in dammaric acids omits C-16 due to its absence.

Dammaric acid B (**8**) is a 19-member ring dammaric acid diterpenoid, isolated as a white powder, with $[\alpha]_D^{25}$ −30 (*c* 0.1, MeOH). ^{1}H NMR analysis revealed a methine-bearing oxygen at δ_H 3.24 (1H, br s, H-3), corresponding to a ^{13}C NMR signal at δ_C 74.2 (C-3) (Tables 1 and 2). In addition, the ^{13}C NMR signal at δ_C 179.7 (C-15)indicated the presence of a carboxyl group. The ion peak of HR-ESI-MS at *m/z* 329.2081 $[M + Na]^+$ (Calcd. for $C_{19}H_{30}O_3Na$, 329.2087), DEPT and ^{13}C NMR spectra revealed 19 carbon atoms, comprising 4 primary carbons, 6 secondary carbons, 4 tertiary carbons, and 5 quaternary carbons. The HMBC from δ_H 0.96 (s, CH_3-17) to δ_C 41.7 (C-13) and subsequently to the carboxyl δ_C 179.7 (C-15) suggests the carboxyl group's position at C-15 (Fig. 2). The NMR data of **8** closely resembles that of the known compound araucarol (**7**), except for the absence of C-16 and the transformation of C-15 from carbonyl (δ_C 215.2) to carboxyl (δ_C 179.7), attributed to oxidative cleavage. NOESY analysis revealed a correlation signal between δ_H 0.84 (s, CH_3-19) and 3.24 (br s, H-3), indicating that 3-OH adopts a β configuration (Fig. 3). The ECD spectrum confirms the absolute configuration of **8** as 3*S*, 5*R*, 9*S*, 10*R*, 13*S* (Fig. 4).

Dammaric acid C (**9**), a white powder with $[\alpha]_D^{25}$ −52 (*c* 0.1, MeOH), possesses the dammaric acid skeleton with 19 carbon atoms, as determined by HR-ESI-MS at *m/z* 305.2106 $[M + H]^+$ (Calcd. for $C_{19}H_{29}O_3$, 305.2111). It exhibits characteristics similar to **3** in the A ring, as evidenced by ^{13}C NMR data (Table 1). Comparison of the ^{13}C NMR signals of **9** and **3** reveals that the sole difference lies in the oxidative cleavage at the C-16 position, with C-15 transforming into a carboxyl group, resulting in an upfield shift from δ_C 214.9 to δ_C 183.9. HSQC, HMBC, and COSY spectra confirm an identical planar structure to **8** (Fig. 2), while NOESY signals (Fig. 3) and ECD spectra (Fig. 4) indicate an absolute configuration of 5*R*, 9*S*, 10*R*, 13*S*, consistent with **8**.

Dammaric acid D (**10**) was isolated as a white powder with a molecular formula of $C_{19}H_{28}O_4$, indicating 6 degrees of unsaturation, as determined by HR-ESI-MS analysis. The spectrum showed a peak at *m/z* 343.1874 $[M + Na]^+$ (Calcd. for $C_{19}H_{28}O_4Na$, 343.1880). Its NMR signals were characterized similarly to the known compound araucarolone (**4**). In the A ring, the ^{13}C NMR signals at δ_C 210.8 and 82.4 indicated the presence of C-2 carbonyl and C-3 hydroxyl structures, respectively, similar to those in **4** (Table 1). HMBS analysis revealed correlations between δ_H 2.61 (d, H-1) and 3.98 (d, H-3) with the carbonyl carbon at δ_C 210.8 (C-2), while δ_H 1.18 (s, CH_3-18) correlated with the hydroxyl carbon at δ_C 82.4 (C-3), further confirming the position of each substituent in the A ring. Additionally, HSQC and COSY signals elucidated the complete molecular planar configuration (Fig. 2). NOESY correlations indicated that the 3-hydroxyl group also has a β configuration (Fig. 3). The specific rotation $[\alpha]_D^{25}$ −18 (*c* 0.1, MeOH) and comparison of measured to calculated ECD spectra values demonstrate that the configuration of **10** is 3*R*, 5*R*, 9*S*, 10*R*, 13*S* (Fig. 4).

Dammaric acid E (**11**), a white powder with $[\alpha]_D^{25}$ −36 (*c* 0.1, MeOH), exhibited an HR-ESI-MS *m/z* of 319.1901 $[M + H]^+$ (Calcd. for $C_{19}H_{27}O_4$, 319.1904). Its structure is characterized similarly to the known compound araucarenolone (**6**) in the A ring, with ^{13}C NMR signals at δ_C 124.0 (C-1), 143.7 (C-2), and 200.7 (C-3) indicating an identical α, β-unsaturated ketone structure (Table 1). The 2D NMR spectral signals elucidated the complete planar structure of the molecule (Fig. 2). NOESY signals revealed a relative configuration consistent with other dammaric acid com-

Table 2 ^{1}H-NMR spectrum (600 MHz) data of new compounds.

Compd.	H-1	H-2	H-3	H-5	H-6	H-7	H-9	H-11	H-12	H-14	H-15	H-16	H-17	H-18	H-19	H-20
1	2.12 m 1.50 td (14.5, 5.1)	2.70 td (14.8, 5.3) 2.28 m	–	1.58 m	2.11 m 1.93 m	5.48 m	1.71 m	1.67 m 1.43 td (14.5, 5.1)	1.73 m 1.55 m	2.23 m 2.13 m	–	2.15 s	1.04 s	1.14 s	1.08 s	1.09 s
2	1.53 m	1.91 m 1.62 m	3.47 t (2.7)	1.56 m	1.88 m 1.94 m	5.46 dd (5.3. 2.2)	1.78 m	1.65 m 1.41 m	1.71 m 1.60 m	2.28 br d (13.9) 2.09 dd (14.1, 2.8)	5.80 dd (17.5, 10.7)	4.39 m	1.06 s	0.95 s	0.96 s	0.89 s
5	2.49 m 1.29 t (13.0)	4.57 m	–	1.55 m	2.16 m 1.94 br d (16.87)	5.50 m	1.78 m	1.69 m 1.48 m	1.73 m 1.62 m	2.28 br d (14.1) 2.13 m	–	4.40 m	1.09 s	1.19 s	1.15 s	1.19 s
8	1.54 m 1.38 m	1.76 m 1.43 m	3.24 br s	1.47 m	1.85 m 1.79 m	5.39 br d (3.1)	1.68 m	1.51 m 1.26 m	1.65 m 1.59 m	2.22 br d (13.9) 2.05 dd (14.3, 2.4)	–	–	0.96 s	0.86 s	0.84 s	0.81 s
9	2.13 m 1.50 td (14.0, 3.9)	2.70 td (14.6, 5.2) 2.27 dt (14.5, 3.6)	–	1.56 dd (12.1, 4.0)	2.08 m 1.94 m	5.48 br d (3.9)	1.75 m	1.65 dt (13.3, 4.0); 1.41 qd (13.1, 3.9)	1.83 m	2.36 br d (14.1) 2.22 br d (14.3, 2.0)	–	–	1.13 s	1.14 s	1.08 s	1.08 s
10	2.61 d (12.8) 2.30 d (12.7)	–	3.98 d (1.3)	1.81 dd (11.4, 4.6)	2.11 m 2.05 m	5.50 br d (3.7)	2.01 br d (2.9)	1.52 td (8.8, 4.2); 1.40 qd (13.1, 4.0)	1.85 m 1.73 td (13.4, 3.8)	2.40 br d (14.1) 2.25 dd (14.3, 2.4)	–	–	1.11 s	1.18 s	0.78 s	0.89 s
11	6.23 s	–	–	1.88 m	2.09 m 1.99 m	5.54 m	1.93 m	1.78 m 1.47 m	1.85 m 1.72 m	2.36 m 2.24 dd (14.3, 2.4)	–	–	1.14 s	1.17 s	1.21 s	1.09 s
12	2.51 br d (16.9) 2.37 d (16.9)	–	–	2.20 m	2.00 m 1.87 m	5.37 br d (4.0)	2.60 br d (11.60)	1.52 m 1.23 m	1.66 m 1.87 m	2.25 m; 2.09 br dd (14.3, 2.0)	–	–	0.97 s	1.17 s	1.10 s	0.91 s
14	1.49 td (13.5, 4.3)	2.70 td (15.2, 4.8) 2.26 dt (13.8, 3.5)	–	1.71 m	2.12 m 1.90 m	5.43 m	1.54 dd (11.2, 4.4)	1.59 m 1.38 m	1.43 m 1.34 m	2.09 m 1.94 m	3.36 dd (9.8, 2.2)	3.77 dd (10.8, 2.0) 3.53 t (11.8)	0.80 s	1.14 s	1.08 s	1.08 s
15	2.60 d (12.8) 2.28 d (12.8)	–	3.97 m	1.79 dd (11.3, 4.7)	2.01–2.09 m	5.44 br d (2.9)	1.96 br s	1.46 br d (3.1) 1.39 m	1.43 m 1.35 m	2.13 m 1.98 br s	3.36 dd (9.4, 2.4)	3.77 dd (10.8, 2.4) 3.52 t (10.2)	0.77 s	1.17 s	0.78 s	0.88 s
16	1.74 dt (13.5, 2.8) 1.08 m	1.44 m	3.01 m	1.02 t (8.4)	1.84–1.90 m	5.30 m	1.54 br s	1.46 br s 1.21 m	1.37 m 1.26 m	1.99 br dd (14.1, 2.0) 1.79 br d (14.3)	3.07 m	3.51 m 3.21 m	0.64 s	0.81 s	0.89 s	0.77 s

*$CDCl_3$: **1**, **2**, **5**, **9**–**11**, **14**, **15**; DMSO-d_6: **8**, **12**, **16**.

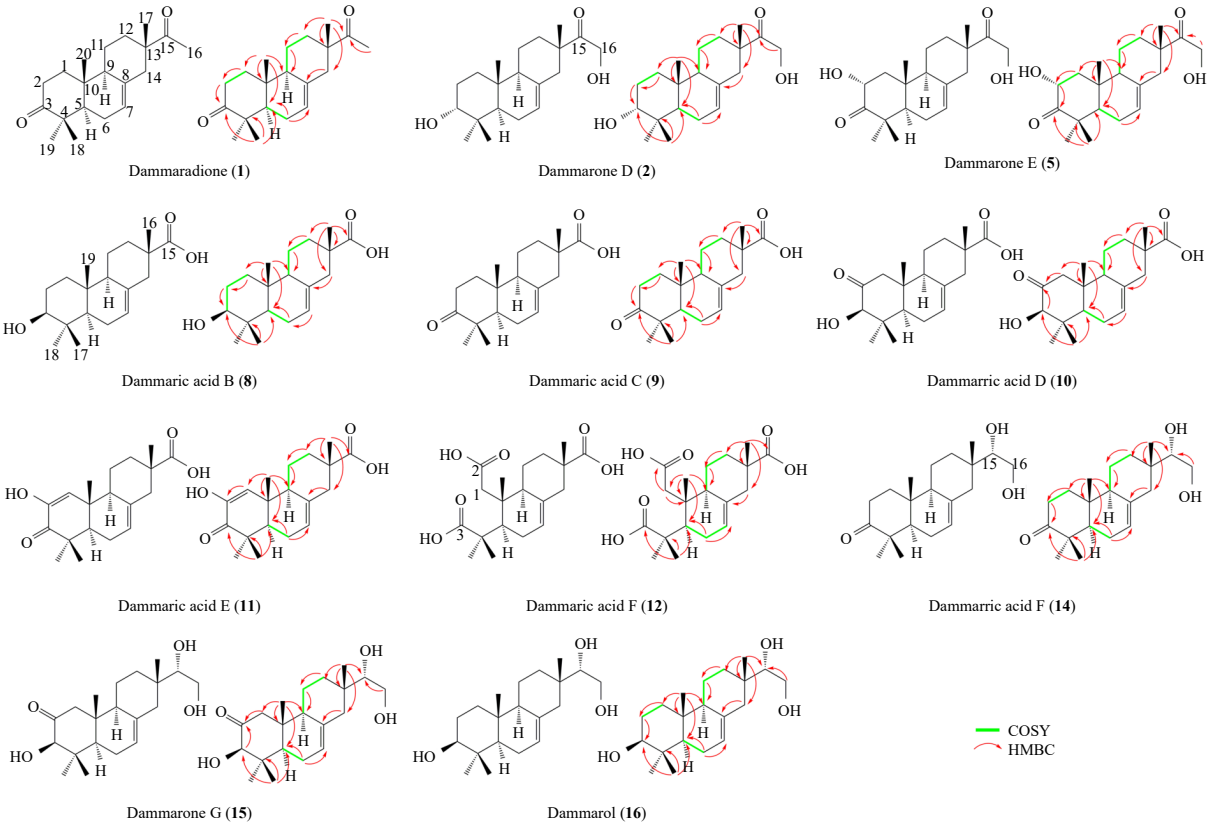

Fig. 2 Molecular structure and 2D NMR signals of new compounds (**1**, **2**, **5**, **8**–**12**, **14**–**16**).

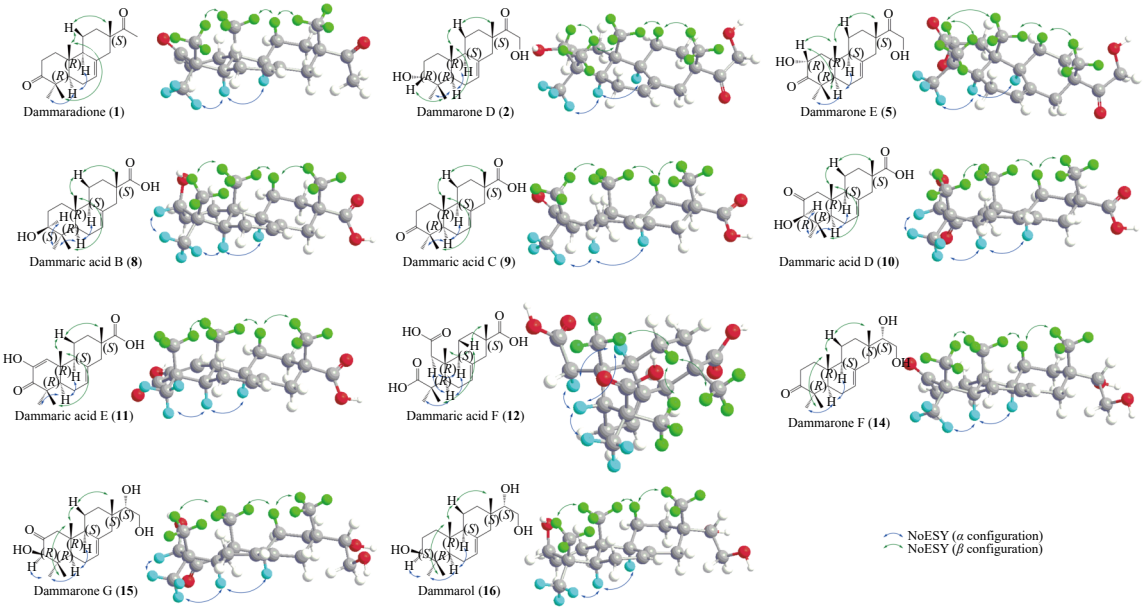

Fig. 3 Molecular structure and NOESY signals of new compounds (**1**, **2**, **5**, **8**–**12**, **14**–**16**).

pounds (Fig. 3), while ECD spectroscopy confirmed the absolute configuration as 5*R*, 9*S*, 10*R*, 13*S* (Fig. 4).

Dammaric acid F (**12**) was obtained as a white powder with 19 carbon atoms, including C-7, 8 double bond signals at δ_C 122.4 and 134.9, similar to those in **8**–**11** (Table 1). The excimer ion peak *m/z* 375.1770 $[M + Na]^+$ (Calcd. for $C_{19}H_{28}O_6Na$, 375.1778) in HR-ESI-MS indicated the presence of 6 oxygen atoms, the highest number among all compounds in this study. Three carboxyl signals were observed in the sp^2 field of the ^{13}C NMR spectrum of **12**, at δ_C 173.9 (C-2), 180.2 (C-3), and 179.7 (C-15). The ^{13}C-NMR signals of the B and C rings are largely consistent with the structure of **9**. However, the specific optical rotation of **12**, $[\alpha]_D^{25}$ +1 (*c* 0.1, MeOH), is nearly racemic compared to other diterpenes with rigid three-ring structures, suggesting an opened A-ring and reduced molecular rigidity. HMBC, HSQC, and COSY analyses determined the positions of the three carboxyl groups and confirmed the ring-opening planar structure (Fig. 2). The A-ring opening caused shifts in δ_H 0.91 (s, CH_3-20), 0.97 (s, CH_3-17), and 1.17 (s, CH_3-18) due to spatial rearrangement, but NOE correlations with δ_H 1.23 (m, H-11β) indicated their common orientation. NOE correlations between H-9 and H-5, and between H-5 and CH_3-19, suggested their opposite orienta-

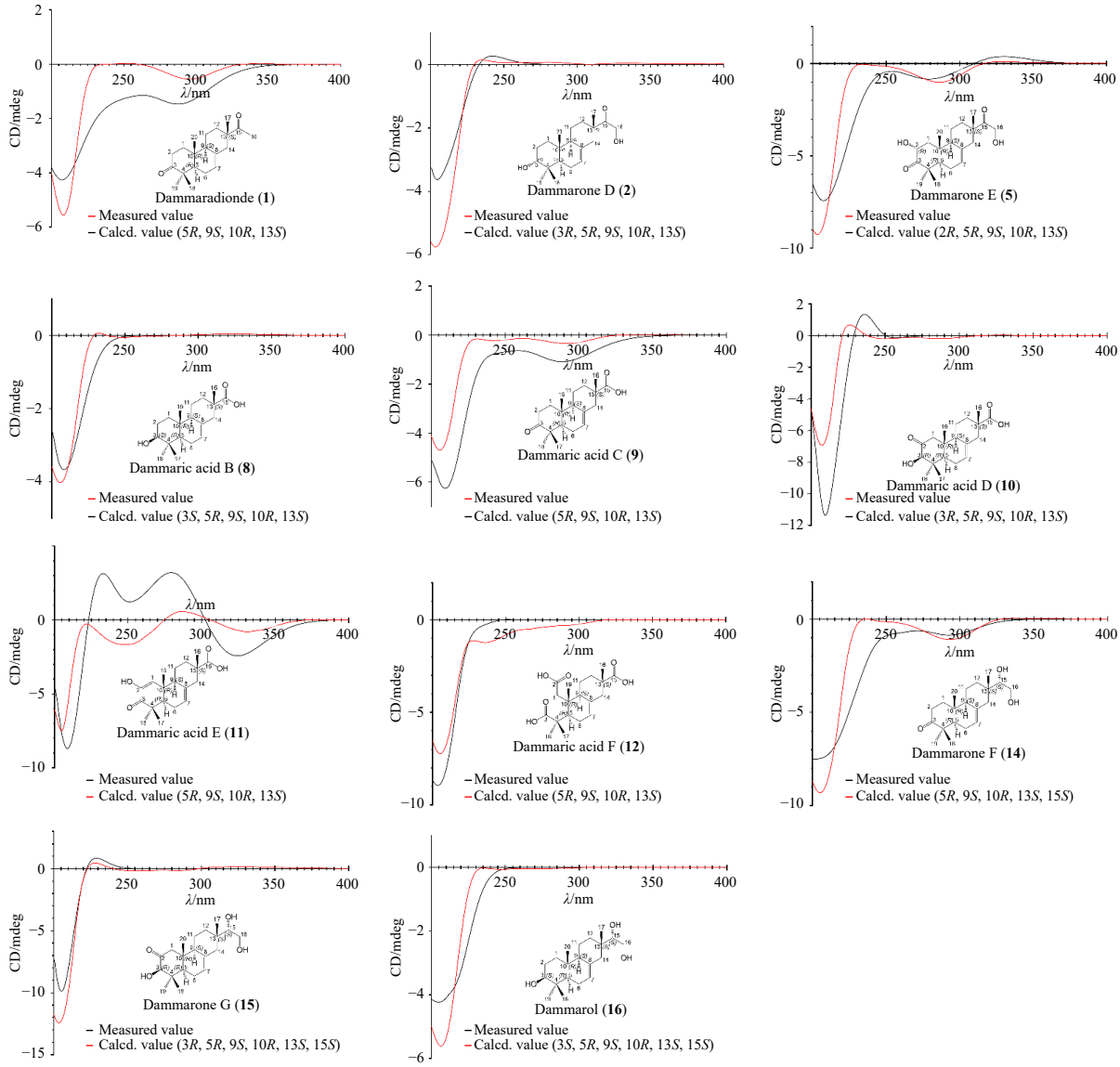

Fig. 4 ECD spectra of new compounds and comparison with calculated values.

tion (Fig. 3). Comparison of the ECD spectrum with calculated values confirms the absolute configuration as 5*R*, 9*S*, 10*R*, 13*S* (Fig. 4).

Dammarone F (**14**) is a 15,16-pimaricol diterpenoid, isolated as a white solid with a specific optical rotation of $[\alpha]_D^{25}$ −48 (*c* 0.1, MeOH). Its molecular formula, $C_{20}H_{32}O_3$, requiring 5 degrees of unsaturation, was determined by HR-ESI-MS *m/z* 321.2420 $[M + H]^+$ (Calcd. for $C_{20}H_{33}O_3$, 321.2424). The ^{1}H NMR spectrum of **14** exhibits a methine and a methylene-bearing hydroxyl groups at δ_H 3.36 (1H, dd, H-15), and at δ_H [3.77(1H, dd) & 3.53(1H, t), H-16] (Table 2), respectively. The ^{1}H-^{1}H COSY spectrum reveals a correlation between these two groups, indicating their linkage (Fig. 2). Furthermore, δ_C 217.2 (C-3) indicates the presence of a carbonyl group (Table 1). The methyl long-range coupling HMBC signals demonstrate that the carbonyl is at C-3 and the -CH(OH)-CH_2OH moiety is at C-15 (Fig. 1). The NMR data of **14** closely resembles that of the known compound (13*S*)-pimar-7-ene-3α,15,16-triol (**13**), with the exception that the C-3 hydroxyl is oxidized to a carbonyl, resulting in a shift of the ^{13}C NMR signal from δ_C 76.2 to δ_C 217.2.

Compound **14** possesses a C-15,16-diol moiety side chain at C-13, and while the entire diterpene molecule exhibits some molecular rigidity due to its intact tricyclic structure, allowing for a notable cotton effect in the ECD spectrum, the side chain remains flexible. This flexibility presents challenges in directly determining the chirality of the C-15 hydroxyl group through ECD spectroscopy. Consequently, we employed Snatzke's method to ascertain the chirality of this hydroxyl group. Snatzke's method, a specialized technique for determining the absolute configuration of vicinal diols, involves forming complexes with dimolybdenum tetraacetate (DT). These complexes yield different cotton effects at specific wavelengths depending on the configurations of the vicinal diol [11]. This approach has been applied to structurally similar pimarene compounds [12]. The absolute configuration of the C-15 hydroxyl group can be determined by observing the cotton effect at 305 nm in the ECD spectrum after mixing the compound with DT. We measured ECD spectra at 0, 20, 40, and 60 minutes after mixing **14** with DT. The resulting complex displayed a positive signal in the 280–350 nm range, which gradually diminished over time, indicating slow dissociation of the complex at room temperature. By subtracting the compound's ECD spectrum from the spectrum with the most prominent cotton effect (0 min), we obtained a diagnostic band (Fig. 5). This band exhibited a positive cotton effect at 305 nm, aligning with literature observations [12] and suggesting that the C-15 hydroxyl group of **14** possesses the *S* configuration.

After confirming the configuration of the flexible C-15 hydroxyl group on the side chain, the remaining chiral groups of **14** are positioned on a rigid molecular framework. NOESY and ECD spectra were utilized to confirm its absolute configuration. Consistent with other compounds in previous sections, the NOESY signals exhibit NOE correlations between δ_H 1.14 (s, CH_3-18), 1.08 (s, CH_3-20), and 0.80 (s, CH_3-17), as well as between 1.08 (s, CH_3-19), 1.71 (m, 5-H), and 1.54 (dd, 9-H) (Fig. 3). A comparison between the experimental and calculated values of the ECD spectra further corroborates its absolute configuration as 5*R*, 9*S*, 10*R*, 13*S*, 15*S* (Fig. 4).

Dammarone G (**15**), also a white powder, $[\alpha]_D^{25}$ −28 (*c* 0.1, MeOH), HR-ESI-MS *m/z* 337.2370 $[M + H]^+$ (Calcd. for $C_{20}H_{33}O_4$, 337.2373), exhibits characteristics similar to **14**. The key distinction lies in the presence of a hydroxyl group attached to C-3 (δ_C 82.4) (Table 1). An NOE correlation between δ_H 3.97 (m, H-3) and 0.78 (s, CH_3-19) indicates that 3-OH is in the *β* configuration (Fig. 3). Applying Snatzke's method, the ECD spectrum intensity of the complex formed by **15** and DT reaches its maximum at 20 min, analogous to compound **14**, displaying a positive signal in the diagnostic band derived from it (Fig. 5). This observation suggests that its C-15 hydroxyl group also adopts the *S* configuration. By integrating data from the NOESY spectrum (Fig. 3) and ECD spectrum (Fig. 4), the absolute configuration of **15** can be established as 3*R*, 5*R*, 9*S*, 10*R*, 13*S*, 15*S*.

Dammarol (**16**), a white powder with $[\alpha]_D^{25}$ −12 (*c* 0.1, MeOH), HR-ESI-MS *m/z* of 323.2578 $[M + H]^+$ (Calcd. for $C_{20}H_{35}O_3$, 323.2581). Its characterization is similar to that of **13**, with identical atomic couplings displayed by HMBC, HSQC, and COSY (Fig. 2). The primary distinction lies in the slight variation of chemical shifts for several carbon atoms near C-3 in the A ring (Table 1, C-3 shifted from δ_C 76.2 in **13** to δ_C 77.5 in **16**). Based on this, it is speculated that **16** and **13** have the same planar structure, and the hydroxyl group on C-3 is isomerized to *β* configuration, which is proved by the NOE correlation between δ_H 0.89 (s, CH_3-19) and 3.01 (m, H-3) in the NOESY signal (Fig. 3). Snatzke's method reveals a positive signal in the diagnostic band, indicating an *S* configuration for the C-15 hydroxyl group of **16** (Fig. 5). The absolute configuration, confirmed by NOESY (Fig. 3) and ECD spectra (Fig. 4), is determined to be 3*S*, 5*R*, 9*S*, 10*R*, 13*S*, 15*S*.

Additional diterpenoids were identified through analysis of their NMR and MS data, as well as by comparison with reported values. These compounds include: araucarone (**3**) [13], araucarolone (**4**) [13], araucarenolone (**6**) [13], araucarol (**7**) [14], and (13S)-pimar-7-ene-3*α*,15,16-triol (**13**) [15]. Notably, although compound **13** has been previously reported, its absolute configuration at the C-15 hydroxyl group had not been established in the literature. To resolve this, Snatzke's method was employed, revealing that the hydroxyl group at C-15 adopts an S configuration (Fig. 5). This assignment is consistent with the stereochemical configuration observed in other C-15,16-diol compounds analyzed in this study.

2.2. Toxicity evaluation

All zebrafish treated with 5 μmol·L^{-1} exhibited no mortality or impaired viability. Araucarone (**3**) and dammaric acid C (**9**), selected for mechanistic studies, demonstrated no toxicity even at a dose of 10 μmol·L^{-1}. These findings indicate the high safety profile of araucarene diterpenes and their derivatives as potential therapeutic agents (Supplementary Fig. S122).

2.3. Hypoglycemic activity of diterpenes

The zebrafish (*Danio rerio*) exhibits glucose metabolism pathways and metabolites similar to those in humans, making it an ideal model for studying the hypoglycaemic activity of drugs [16, 17]. This study utilized a *Tg(Ins:htBid$^{TE\text{-}ON}$; LR)* pancreatic *β* cell ablation zebrafish model [18] to induce hyperglycaemic symptoms. In this transgenic zebrafish, the truncated human Bid protein (htBid) was derived from an insulin promoter and controlled under a tetracycline- and ecdysone-inducible system. Following induction with doxycycline (Dox) and tebufenozide (Tbf), the proapoptotic tBid expression in *β* cells resulted in their apoptosis, which was labeled by the transgenic line *Tg(−1.2ins:H2B-mcherry)*. The zebrafish were subsequently incubated with compounds **1**–**16** and the positive control drug rosiglitazone (RGZ) at 5 μmol·L^{-1} for 24 h for activity testing (Fig. 6A).

The free glucose level was significantly elevated following *β* cell ablation compared to non-induced transgenic zebrafish, indicating that *β* cell ablation induced hyperglycemia in the zebrafish model. The results demonstrated that, in addition to compounds **1** and **13**–**16**, other araucarene diterpenes exhibited blood sugar reduction effects in zebrafish. Compounds **3**, **5**–**9**, **11**–**12** displayed the most significant hypoglycemic activity, comparable to that of the positive control drug RGZ (P <0.001, Fig. 6B). Among them, the half maximal effect concentrations (EC_{50}) of araucarene (**3**) and dammaric acid C (**9**) were evaluated and they were 2.83 ± 0.28, and 3.00 ± 0.31 μmol·L^{-1} (Fig. 6C).

The structure-activity relationship was analyzed based on the presented data (Fig. 6D). The side chain of the C ring at C-13 significantly influenced the activity. The classical araucarene structure, featuring a C-15 carbonyl and C-16 hydroxyl, demonstrated substantial hypoglycemic activity. Similarly, the dammaric acid structure, characterized by C-16 oxidation and fracture, along with a C-15 carboxyl group, exhibited comparable efficacy. However, acetyl or ethanediolyl substitution at C-13 considerably diminished the hypoglycemic activity. Oxidation of the A ring to form a C-2 carbonyl negatively impacted the activity. The configuration of the C-3 hydroxyl also played a crucial role in determining activity, with the *α*-hydroxyl configuration being preferred. Additionally, the presence of a C-3 carbonyl group enhanced the activity.

2.4. Exploration of the hypoglycemic mechanism

To investigate the hypoglycemic mechanisms of araucarene diterpenoids and their derivatives, araucarene (**3**) and dammaric acid C (**9**) were selected for further study. This selection was based on their high abundance in the *A. dammara* extract, significant hypoglycemic activity, and their distinct representation of typical araucarene and dammaric acid, respectively. Notably, compound **9** is a novel discovery. The inhibition of blood glucose elevation primarily involves two mechanisms in different tissues: enhancing glucose uptake in peripheral tissue and promoting regeneration of pancreatic *β* cells. To elucidate the hypoglycemic mechanism, two zebrafish models were employed.

2.4.1. Regulation on glucose uptake

2-NBDG, a fluorescently labeled deoxyglucose analog, was introduced into the zebrafish culture medium to indicate glucose uptake [19]. As illustrated in Fig. 7A, both compounds **3** and **9** significantly promoted glucose uptake to the level of the control group. However, their promotional effect was notably less pronounced than that of RGZ.

2.4.2. Regeneration of pancreatic *β* cells

A double transgenic zebrafish model, *Tg(Ins:htBid$^{TE\text{-}ON}$; LR); Tg (Ins:H2Bmcherry)*, was employed to quantify *β* cells following compound treatment. The *Tg(Ins:H2Bmcherry)* zebrafish expresses red fluorescent protein (mCherry) in *β* cells under the control of an insulin-specific promoter, enabling their labeling. This allows for the observation, quantification, and imaging of zebrafish pancreatic *β* cells *via* fluorescence microscopy [17]. In

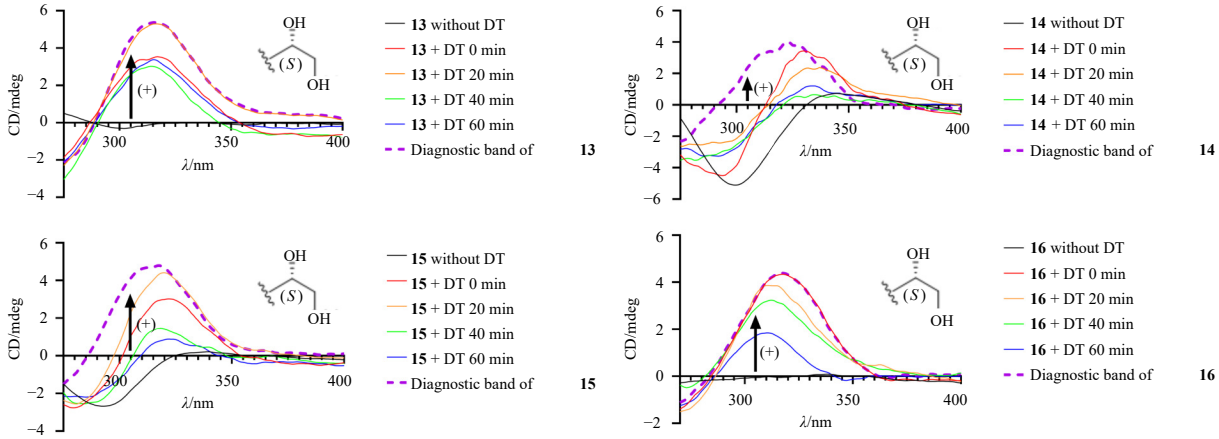

Fig. 5 Determination of absolute configuration of the 15,16-diol moiety of **13**–**16** using Snatzke's method (Diagnostic band: The ECD spectral band of the complex formed by the compound and DT with the largest cotton effect subtracted the ECD spectral band of the compound itself).

comparison to the *β* cell ablation group (tBid + Dox + Tbf + dimethyl sulfoxide (DMSO)], the number of pancreatic *β* cells in the hyperglycaemic zebrafish model increased significantly after 24-h treatment with compounds **3** and **9** (Fig. 7B). These findings suggest that the hypoglycemic activity of *A.dammara* araucarene diterpenoids and derivatives may also be attributed to the promotion of pancreatic *β* cell regeneration (Fig. 7C).

2.4.3. Mechanism on the regeneration of pancreatic β cells

To elucidate the regeneration source of pancreatic *β* cells, three transgenic zebrafish lines *Tg(Mnx1:eGFP)*, *Tg(Ins:Fucci;LR)*, *Tg (gcga:eGFP)* were crossed with the double transgenic zebrafish *Tg(Ins:htBid$^{TE\text{-}ON}$, Ins:H2Bmcherry)* as described in our previous report [17]. Motor neuron and pancreatic homeobox 1 (Mnx1) of *Tg(Mnx1:eGFP)* is a crucial regulatory factor in the early stages of pancreatic differentiation and serves as a marker for PEP cells [20]. The Fucci in *Tg(Ins:Fucci;LR)* functions as a *β* cell cycle sensor in zebrafish, specifically expressing mAG-zGeminin in pancreatic islets. Geminin, a protein specific to the S/G_2/M phase of cell replication, when fused with the monomeric Azami green (mAG) protein, causes *β* cells in the S/G_2/M replication phase to emit green fluorescence, directly indicating new *β* cell replication [21]. The *Tg (gcga:eGFP)* line marks *α* cells with GFP driven by glucagon promoter [17]. These three green fluorescent-labeled zebrafish strains correspond to the three potential sources of regenerated *β* cells: PEP cells, self-replicating *β* cells, and *α* cells. Through microscopic imaging of red fluorescently labeled pancreatic *β* cells and quantification of double-positive cells co-expressing red and green fluorescence, the source of *β* cell regeneration can be determined as PEP cell differentiation, *β* cell self-replication, or *α* cell transdifferentiation, respectively (Fig. 6A).

Following 24-h treatment with compounds **3** and **9**, a significant increase was observed in the number of *β*/PEP double-positive cells co-expressing insulin and Mnx1 fluorescence (Figs. 8A and 8B). However, no statistically significant difference was noted in the number of *β*/self-replicating *β* double-positive cells co-expressing insulin and Fucci fluorescence (Figs. 8C and 8D), nor in *β*/*α* double-positive cells co-expressing insulin and gcga fluorescence (Figs. 8E and 8F). The proportion of *β* cells derived from different cell types was calculated based on these cell counts (Fig. 8G). It was found that the proportion of *β* cells derived from PEP cells in the hyperglycaemic zebrafish model after drug treatment was significantly increased compared with the modeling group (DMSO), and it was the main source of *β* cells (> 60%). In contrast, the proportion of *β* cells derived from self-replicating *β* cells was reduced, while the proportion derived from transdifferentiated *α* cells was not significantly different and accounted for only a small proportion (< 20%). The above results show that **3** and **9** exert hypoglycemic biological activity by promoting the differentiation of PEP cells into *β* cells.

3. Experimental

3.1. General experimental procedures

Optical rotations were measured using a JASCO P-200 polarimeter (Tokyo, Japan). UV spectra were recorded in methanol with a Shimadzu UV-260 spectrophotometer (Kyoto, Japan). ECD spectra were obtained using a JASCO J-810 spectrometer (Tokyo, Japan). IR measurements were performed on a Perkin-Elmer 683 spectrometer. NMR experiments were conducted on Bruker Avance III-600 MHz spectrometers in $CDCl_3$ and DMSO-d_6. HR-ESI-MS data were acquired using a Thermo Fisher Q-Exactive mass spectrometer (Boston, USA). Column chromatography (CC) separations were carried out using silica gel (300–400 mesh; Qingdao Haiyang Chemical Co., Ltd., Qingdao, China) and ODS RP-C_{18} (40–63 μm, FuJi, Aichi, Japan). An Agilent 1260 series system (California, USA) with a COSMOSIL 5C_{18}-MS-Ⅱ (5 μm, 4.6 mm × 150 mm, Kyoto, Japan) column was utilized for high-performance liquid chromatography (HPLC) analysis. Preparative HPLC was performed using a Welch Sail 1000 series instrument equipped with a Welch Ultimate XB-C_{18} column (5 μm, 250 mm × 21.2 mm, China).

3.2. Plant material

The dried wood of *Agathis dammara* (Lamb.) Rich was obtained from Xiamen Garden Botanical Garden (24°26'54.6"N 118°06'26.4"E) in March 2021, located in Xiamen City, Fujian Province, China. A voucher specimen (No. 2021BKS) was preserved in the School of Pharmaceutical Sciences, Xiamen University, and identified by Associate Prof. Quancheng Chen.

3.3. Extraction and isolation

A quantity of 1 kg of dried *A. dammara* wood underwent extraction and refluxing thrice with 2 L of 95% ethanol for 1.5 h, yielding 367 g of concentrated extract. This extract was subsequently suspended in water and extracted with an equal volume of dichloromethane, resulting in 100 g of dichloromethane extract (Fr. A). Initial separation was performed using silica gel column chromatography (petroleum ether-ethyl acetate 100∶1–0∶1), yielding seven fractions (Fr. A1–Fr. A7).

Following HPLC-DAD and thin layer chromatography (TLC)

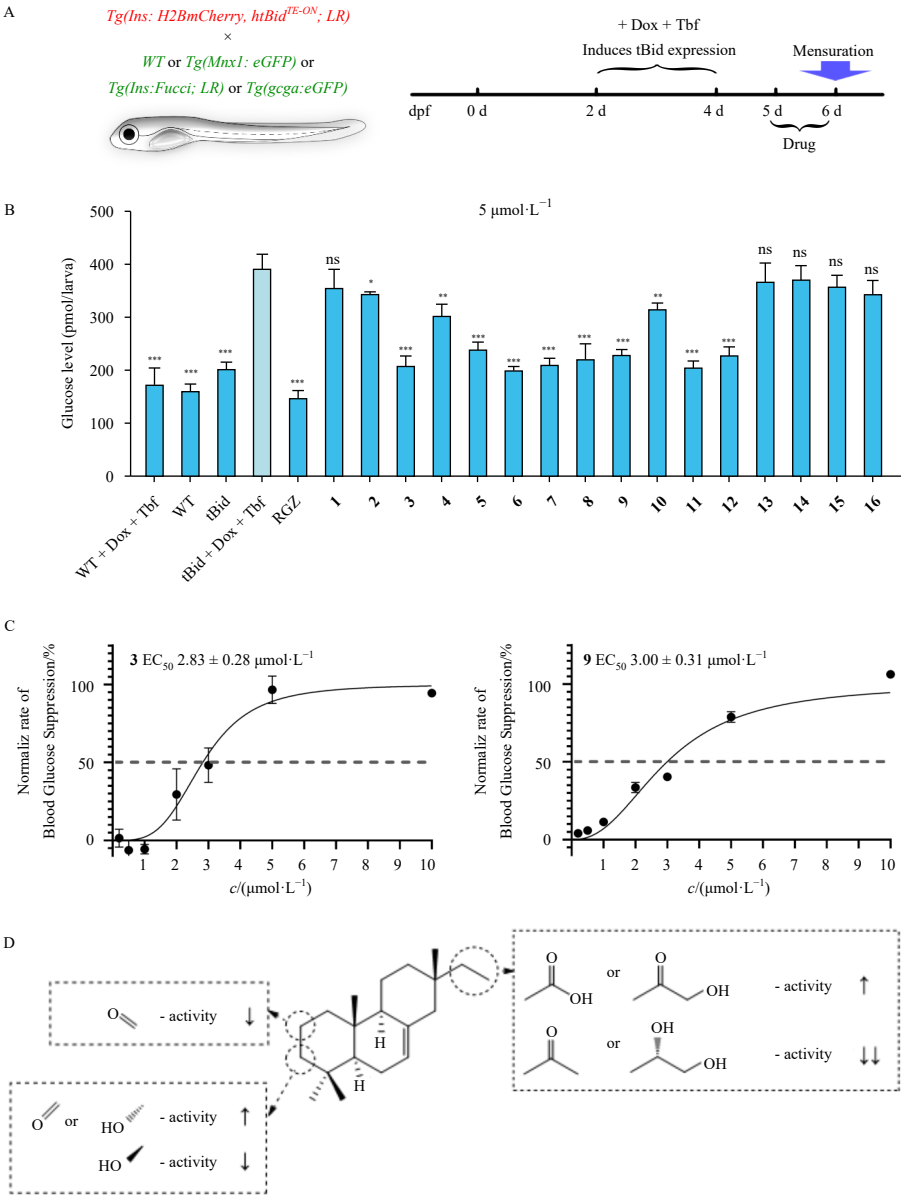

Fig. 6 Biological test of araucarene diterpenoids of *A. dammara* on hypoglycemic activity in zebrafish. (A) Modeling and drug administration of hyperglycaemic zebrafish model. (B) Compound **1**–**16** (5 μmol·L^{-1}) on the change of blood glucose value of zebrafish after 24 h treatment in hyperglycaemic zebrafish model *Tg* (*Ins:htBid* $^{TE\text{-}ON}$ *;LR*). (C) Dose-efficacy curve and EC_{50} of hypoglycemic activity of compounds **3**, **9** on zebrafish. (D) The structure-activity relationship between structure and hypoglycemic activity of compounds **1**–**16** ($^{*}P < 0.05$, $^{**}P < 0.01$, and $^{***}P < 0.001$ *vs* model groups tBid + Dox + Tbf).

analysis, a scheme for further separation of Fr. A3–Fr. A6 was established. This scheme involved off-line separation combining reversed-phase and normal-phase open chromatographic columns, along with preparative HPLC. Initially, each component was passed through Chromatorex C_{18} as the chromatographic stationary phase, with gradient elution performed using conditions determined by HPLC analysis (MeOH/Water, 5%–100%). The eluted components underwent TLC analysis, utilizing dichloromethane and methanol as developing solvents. A developing solvent formula with an R_f value of 0.2–0.3 on TLC served as the mobile phase for silica gel column chromatography separation. The purity of the separated components was verified by TLC and HPLC, with further purification by preparative HPLC performed if necessary (Fig. S1).

Dammaradione (**1**): white powder; melting point: 88.8–91.3 °C; $[\alpha]_D^{25}$ −10 (*c* 0.1 MeOH); UV (MeOH) λ_{max} (log ε) 206 (0.36) nm; IR ν_{max} 2924, 1702, 1455, 1377, 1096 cm^{-1}; HR-ESI-MS *m/z* 303.2317 [M + H]$^+$ (Calcd. for $C_{20}H_{31}O_2$, 303.2319); ^{1}H and ^{13}C NMR data (Tables 1 and 2).

Dammarone D (**2**): white powder; melting point: 108.9–110.0 °C; $[\alpha]_D^{25}$ −24 (*c* 0.1 MeOH); UV (MeOH) λ_{max} (log ε) 209 (0.41) nm; IR ν_{max} 3852, 3741, 3434, 2926, 1703, 1456, 1388, 1218, 1227, 1051, 998 cm^{-1}; HR-ESI-MS *m/z* 321.2422 [M + H]$^+$ (Calcd. for $C_{20}H_{33}O_3$, 321.2424); ^{1}H and ^{13}C NMR data (Tables 1 and 2).

Dammarone E (**5**): white powder; melting point: 139.6–141.3 °C; $[\alpha]_D^{25}$ −22 (*c* 0.1 MeOH); UV (MeOH) λ_{max} (log ε) 206 (0.36) nm; IR ν_{max} 3461, 3365, 2923, 1706, 1454, 1387, 1265, 1102, 997 cm^{-1}; HR-ESI-MS *m/z* 335.2215 [M + H]$^+$ (Calcd. for $C_{20}H_{31}O_4$, 335.2217); ^{1}H and ^{13}C NMR data (Tables 1 and 2).

Dammaric acid B (**8**): white powder; melting point: 208.2–210.3 °C; $[\alpha]_D^{25}$−30 (*c* 0.1 MeOH); UV (MeOH) λ_{max} (log ε) 208 (0.38) nm; IR ν_{max} 3852, 3744, 3672, 3616, 3380, 2931, 1697, 1521, 1459, 1385, 1230, 1120, 1042, 979, 930 cm^{-1}; HR-ESI-MS *m/z* 329.2081 [M + Na]$^+$ (Calcd. for $C_{19}H_{30}O_3Na$, 329.2087); ^{1}H and ^{13}C NMR data (Tables 1 and 2.

Dammaric acid C (**9**): white powder; melting point: 161.7–165.5 °C; $[\alpha]_D^{25}$ −52 (*c* 0.1 MeOH); UV (MeOH) λ_{max} (log ε)

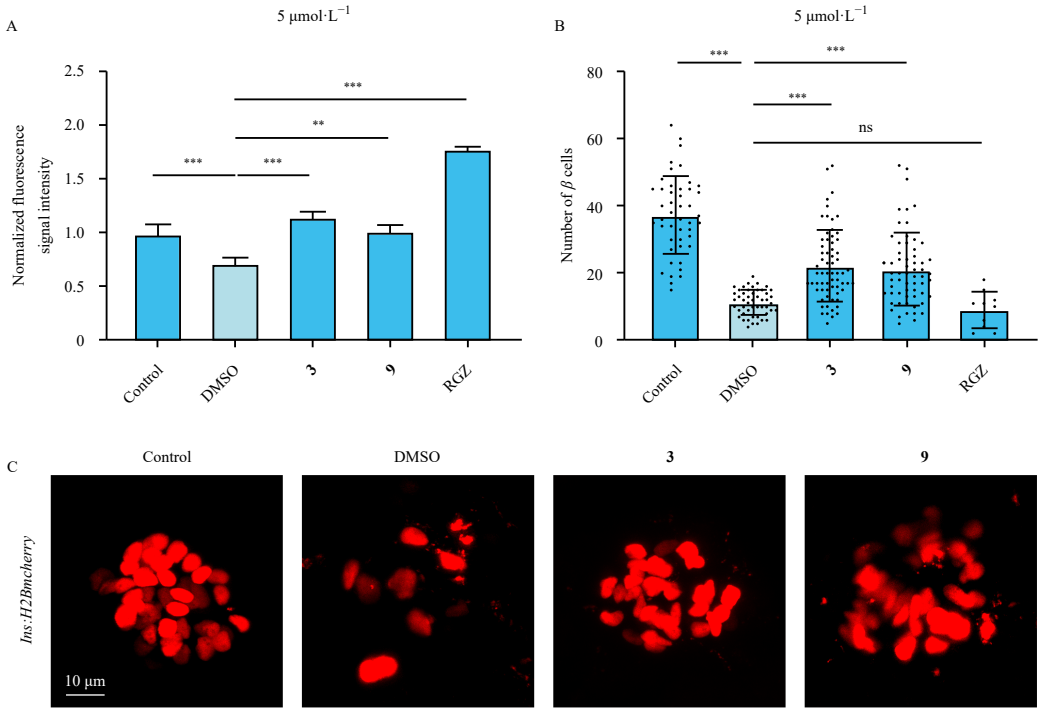

Fig. 7 Preliminary mechanism of compounds **3**, **9** on hypoglycemic activity in zebrafish. (A) Change in fluorescence value of hyperglycaemic zebrafish model after 24 h treatment of compounds **3**, **9** (5 μmol·L^{-1}) in medium containing 600 μmol·L^{-1} glucose analog probe 2-NBDG for 3 h. (B)(C) Count and imaging of islets *β* cells in a hyperglycaemic zebrafish model after 24 h of treatment with compounds **3**, **9** (5 μmol·L^{-1}), characterized by mCherry-labeled insulin-specific promoter *Tg(Ins:H2BmCherry)* ($^{*}P$ < 0.05, $^{**}P$ < 0.01, and $^{***}P$ < 0.001 *vs* model groups tBid + Dox + Tbf + DMSO).

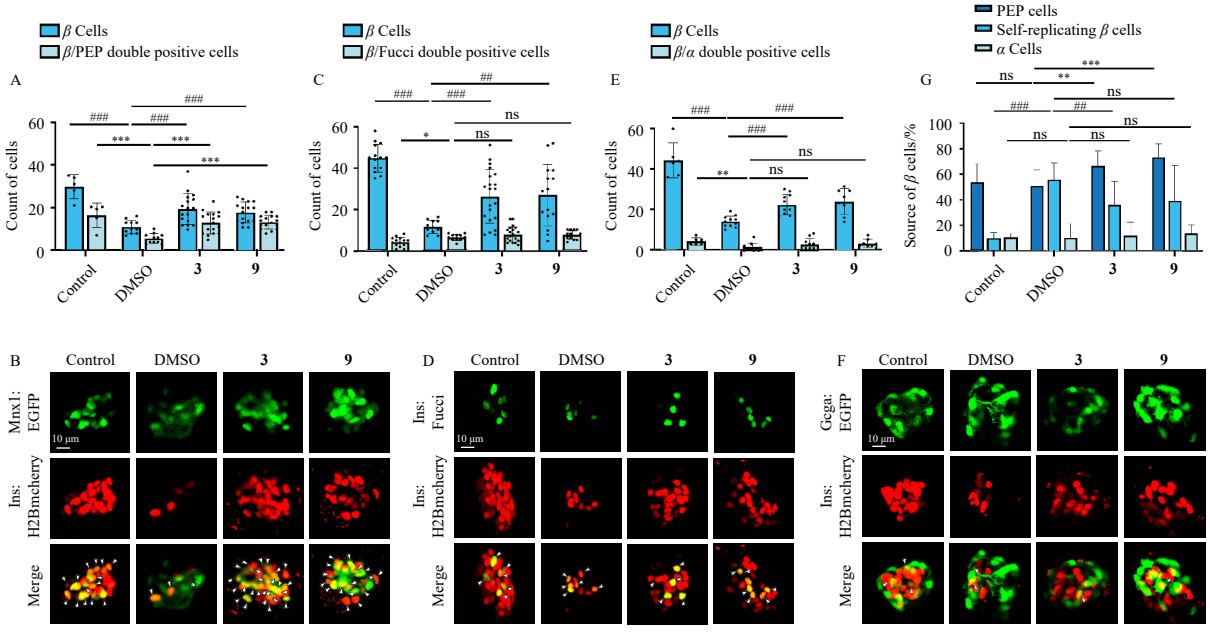

Fig. 8 Mechanism study of compounds **3**, **9** on pancreatic *β* cell regeneration in the hyperglycaemic zebrafish model. Count and microscopic imaging of *β* cells (red cells) and double-positive cells (yellow cells) in hybridization between different strains of zebrafish models and *Tg(Ins:htBid$^{TE\text{-}ON}$, Ins:H2Bmcherry)* after 24 h of compounds 3, 9 treatment. (A and B) *Tg(Mnx1:eGFP)* (green cells) (C and D) *Tg(Ins:Fucci;LR)* (green cells) (E and F) *Tg(gcga:EGFP)* (green cells) (G) Proportion of *β* cells derived from different cells after treatment by **3**, **9** ($^{*/\#}P$ < 0.05, $^{**/\#\#}P$ < 0.01, and $^{***/\#\#\#}P$ < 0.001 *vs* model groups tBid + Dox + Tbf + DMSO).

207 (0.37) nm; IR ν_{max} 3852, 3743, 3673, 3625, 2961, 1699, 1521, 1460, 1387, 1276, 1120 cm^{-1}; HR-ESI-MS *m/z* 305.2106 [M + H]$^{+}$ (Calcd. for $C_{19}H_{29}O_3$, 305.2111); ^{1}H and ^{13}C NMR data (Tables 1 and 2).

Dammaric acid D (**10**): white powder; melting point: 188.4–190.0 °C; $[\alpha]_D^{25}$ −18 (*c* 0.1 MeOH); UV (MeOH) λ_{max} (log ε) 206 (0.34) nm; IR ν_{max} 3417, 2966, 1707, 1455, 1387, 1267, 1214, 1110 cm^{-1}; HR-ESI-MS *m/z* 343.1874 [M + Na]$^{+}$ (Calcd. for $C_{19}H_{28}O_4Na$, 343.1880); ^{1}H and ^{13}C NMR data (Tables 1 and 2).

Dammaric acid E (**11**): white powder; melting point: 152.1–158.8 °C; $[\alpha]_D^{25}$ −36 (*c* 0.1 MeOH); UV (MeOH) λ_{max} (log ε) 206 (0.39), 267 (0.39) nm; IR ν_{max} 2926, 1699, 1459, 1403, 1275, 1222 cm^{-1}; HR-ESI-MS *m/z* 319.1901 [M + H]$^{+}$ (Calcd. for $C_{19}H_{27}O_4$, 319.1904); ^{1}H and ^{13}C NMR data (Tables 1 and 2).

Dammaric acid F (**12**): white powder; melting point: 218.7–221.4 °C; $[\alpha]_D^{25}$ 1 (*c* 0.1 MeOH); UV (MeOH) λ_{max} (log ε) 204 (0.09) nm; IR ν_{max} 3746, 2929, 1706, 1521, 1461, 1402, 1274, 883 cm^{-1}; HR-ESI-MS *m/z* 375.1770 [M + Na]$^{+}$ (Calcd. for $C_{19}H_{28}O_6Na$, 375.1778); ^{1}H and ^{13}C NMR data (Tables 1 and 2).

Dammarone F (**14**): white powder; melting point:

139.0–141.8 °C; $[\alpha]_D^{25}$ −48 (*c* 0.1 MeOH); UV (MeOH) λ_{max} (log ε) 207 (0.35) nm; IR ν_{max} 2939, 3338, 2953, 1705, 1516, 1456, 1383, 1205, 1071 cm^{-1}; HR-ESI-MS *m/z* 321.2420 $[M + H]^+$ (Calcd. for $C_{20}H_{32}O_3$, 321.2424); ^1H and ^{13}C NMR data (Tables 1 and 2).

Dammarone G (**15**): white powder; melting point: 129.5–132.7 °C; $[\alpha]_D^{25}$ −28 (*c* 0.1 MeOH); UV (MeOH) λ_{max} (log ε) 208 (0.41) nm; IR ν_{max} 3399, 2959, 1713, 1446, 1387, 1268, 1213, 1099, 1063, 1015 cm^{-1}; HR-ESI-MS *m/z* 337.2370 $[M + H]^+$ (Calcd. for $C_{20}H_{33}O_4$, 337.2373); ^1H and ^{13}C NMR data (Tables 1 and 2).

Dammarol (**16**): white powder; melting point: 179.9–182.2 °C; $[\alpha]_D^{25}$ −12 (*c* 0.1 MeOH); UV (MeOH) λ_{max} (log ε) 207 (0.28) nm; IR ν_{max} 3315, 2932, 1520, 1456, 1382 cm^{-1}; HR-ESI-MS *m/z* 323.2578 $[M + H]^+$ (Calcd. for $C_{20}H_{35}O_3^+$, 323.2581); ^1H and ^{13}C NMR data (Tables 1 and 2).

3.4. ECD calculations

Conformational analyses were conducted using Schrodinger Maestro 12.8's Conformational Search function. The resulting conformers were subsequently optimized using the OPLS4 force field and filtered with an RMSD threshold of 0.1 Å and an energy window of 5.02 kcal·mol^{-1}. Conformations accounting for less than 1% of the Boltzmann distribution at room temperature were eliminated. The five conformations with energies closest to the lowest energy conformation were selected for excitation spectrum calculations. Theoretical calculations were performed using Gaussian 09W. The chosen conformers were ultimately optimized at the B3LYP/6-31G(d) level in methanol.

The ECD calculations for the selected conformers were performed in methanol using Time-dependent Density functional theory (TD-DFT) at the B3LYP/6-31 + G (d) or B3LYP/6-311 + G (d, p) level, utilizing Gaussian 09W. Rotatory strengths for 20 or 30 excited states were computed. Subsequently, GaussView 6.0 was employed to generate the spectrum by combining the energies of various conformations according to the Boltzmann energy equation, resulting in the final ECD calculation spectrum.

3.5. Establishment and treatment of hyperglycaemic zebrafish model

Following the crossbreeding of the transgenic zebrafish strain *Tg (Ins:htBid$^{TE\text{-}ON}$, Ins:H2Bmcherry)* with the desired genotype strain, fertilized eggs were collected the subsequent day, which was designated as day 0 post-fertilization (0 dpf). Tbf (3 μL, 50 mmol·L^{-1}) and Dox (3 μL, 100 mmol·L^{-1}) were introduced into a 3.5 cm cell culture dish containing 6 mL of 0.3 × Danieau's buffer. Subsequently, the dish was incubated in a zebrafish incubator under dark conditions for 48 h to induce *β* cell ablation at 2 dpf.

Diabetic zebrafish that were ready to be used in experiments after *β* cell ablation were rinsed with 0.3 × Danieau's buffer to remove Tbf and Dox. The larvae were placed into a 24-well plate at a density of 10 zebrafishes/well in 2 mL of egg water. All compounds were made in mmol·L^{-1} with DMSO (prepare other concentrations when calculating EC_{50}). For the treatment, each group was added accordingly with 2 mL of egg water treated with 1 μL of each of the compounds (10 mmol·L^{-1}) to reach the final concentration of (5 μmol·L^{-1}), and the control group was treated with the same amount of DMSO. The treatments lasted for 24 h in the zebrafish incubator. The group of tBid, which was not induced with Tbf and Dox, was used as a control of normal zebrafish.

3.6. Total glucose level test

Following compound treatment, a pool of 10 larvae was homogenized in 100 μL of sample buffer. The homogenate was centrifuged at 10 000 r·min^{-1} for 10 min. Free glucose in 10 μL of supernatant (equivalent to one larva) was quantified according to the manufacturer's protocol. Fluorescence (excitation, 520 nm; emission, 580–640 nm) was measured using a SpectraMax M5 Microplate Reader (Molecular Devices, California, USA). Each sample was analyzed for three pools. The resultant data were imported into GraphPad Prism 8.0.2 software, and statistical differences among the groups were evaluated using the *t*-test method.

3.7. 2-NBDG test

Following compound administration, zebrafish (6 dpf) were incubated in a culture medium containing 600 μmol·L^{-1} 2-NBDG (Apexbio, B6035, Texas, USA) for 3 h. A group of 5 larvae was homogenized in 100 μL of sample buffer. The homogenate was centrifuged at 10 000 r·min^{-1} for 10 min. The supernatant (30 μL) was transferred to a 96-well plate for fluorescence detection (excitation, blue 475 nm; emission, 500–550 nm) using a SpectraMax M5 Microplate Reader (Molecular Devices, California, USA). Each sample was measured in triplicate. The resulting data were analyzed using GraphPad Prism 8.0.2 software, and statistical differences between groups were evaluated using the *t*-test method..

3.8. Microscopic imaging and counting of pancreatic cells

After 24 h of compound treatment, the larvae were washed with 0.3 × Danieau's buffer. The specimens were then fixed overnight in 4% paraformaldehyde at 4 °C. Subsequently, the larvae were mounted on slides using aqua-mount (Richard-Allan-Scientific, Michigan, USA), with their right sides facing upwards to expose the islets. Cell counting was performed based on RFP and GFP signals using a Leica TCS SP8 microscope (Leica, Wetzlar, Germany) with a 63 × objective lens. Image processing and cell counting were conducted using LASX Office 1.4.5 software. The resulting data were analyzed using GraphPad Prism 8.0.2 software, and statistical differences between groups were assessed using the *t*-test method.

3.9. Determination of absolute configuration of the 15,16-diol moiety using Snatzke's method

Following the established protocol [12], approximately 1∶1 mixtures of DT were prepared using 1.0 mg·L^{-1} of compounds **13–16**. Immediately after mixing, the initial CD spectrum was recorded, and its progression was monitored until it reached a stationary state (0, 20, 40, 60 min). The sign of the characteristic band at 305 nm (band IV, as per Snatzke's nomenclature) correlates with the absolute configuration of the 15,16-diol moiety.

4. Conclusion

This study characterizes araucarene as a series of diterpene compounds extracted from plants in the Araucariaceae family. Its potential biological activity has been largely overlooked, with only basic chemical structure studies conducted in the 1960s [6, 7]. Araucarene is distinguished by a diterpene framework featuring pimarene, with varying degrees of oxidation observed on its side chain at C-13 and the A ring. The most common configuration involves a side chain substitution at C-15 with a carbonyl group and at C-16 with a hydroxyl group, as exemplified by compounds such as araucarone, araucarolone, and araucarol. This research identifies a series of derivatives with novel structures, including C-16 methyl substitution (**1**), the dammaric acid structure of C-16 oxidative cleavage (**8–12**), and the dammarol structure of C-15 and 16 hydroxyl groups (**13–16**). Various degrees of oxidation have occurred on the A-ring of these compounds, including a novel

structure where the entire A-ring is oxidized and cleaved into two carboxyl groups (**12**). Notably, the dammaric acid structure exhibits hypoglycemic biological activity comparable to that of classical araucarene and demonstrates the same hypoglycemic mechanism.

In summary, 11 new abietene and pimarene diterpenes along with 15 known analogs were isolated from *A. dammara*. These araucarene diterpenes and derivatives with different structural characteristics exhibit different hypoglycemic activities in the hyperglycaemic zebrafish model. On this basis, the structure-activity relationship of these drugs was analyzed. Further mechanism studies revealed that these drugs produce hypoglycemic activity mainly by promoting pancreatic β cell regeneration and glucose uptake. The mechanism by which the drugs promote pancreatic β cell regeneration is to promote the differentiation of PEP cells into β cells in zebrafish. These findings enrich the structural diversity of araucarenes and provide potential lead compounds for the development of naturally derived anti-hyperglycaemic drugs.

Funding

This work was supported by the Traditional Chinese Medicine Foundation of Xiamen City, China (No. XWZY-2023-0303) and the Natural Science Foundation of Xiamen City, China (No. 3502Z20227162).

Supporting Information

NMR, HR-ESI-MS, IR, UV, ECD spectra of new compounds, as well as toxicity and activity data of compounds **1**–**16** can be requested by sending E-mail to the corresponding authors.

Declaration of Competing Interest

These authors have no conflict of interest to declare.

References

1 Ahda M, Jaswir I, Khatib A, et al. A review on selected herbal plants as alternative anti-diabetes drugs: chemical compositions, mechanisms of action, and clinical study. *Int J Food Prop*. 2023;26(1):1414-1425. https://doi.org/10.1080/10942912.2023.2215475.
2 Ma X, Nan F, Liang HT, et al. Excessive intake of sugar: an accomplice of inflammation. *Front Immunol*. 2022;13:988481. https://doi.org/10.3389/fimmu.2022.988481.
3 Rippe JM, Angelopoulos TJ. Fructose-containing sugars and cardiovascular disease. *Adv Nutr*. 2015;6(4):430-439. https://doi.org/10.3945/an.114.008177.
4 Xue HK, Hao ZT, Gao YC, et al. Research progress on the hypoglycemic activity and mechanisms of natural polysaccharides. *Int J Biol Macromol*. 2023;252:126199. https://doi.org/10.1016/j.ijbiomac.2023.126199.
5 Setoguchi H, Asakawa OT, Pintaud JC, et al. Phylogenetic relationships within Araucariaceae based on *rbcL* gene sequences. *Am J Bot*. 1998;85(11):1507-1516. https://doi.org/10.2307/2446478.
6 Enzell CR, Thomas BR. The wood resin of *Agathis australis* Salis. Structure and stereochemistry of the main constituents. *Tetrahedron Lett*. 1964(7-8):391-397.
7 Enzell CR, Thomas BR. The chemistry of order araucariales. 2. Wood resin of *Agathis australis*. *Acta Chem Scand*. 1965;19(4):913-919.
8 Wang AY, Yue SS, Peng AK, et al. A review of research progress on agathis dammara and its application prospects for cardiovascular diseases and fatty liver disease. *Mini-Rev Med Chem*. 2021;21(6):670-676. https://doi.org/10.2174/1389557520666201117110834.
9 Di X. Damar minyak of *Agathis*. *Furniture Interior Design*. 2013;(12):90-93.
10 Zhang QY, Cai ZY, Yu ZW, et al. *Agathis dammara* extract and its monomer araucarone attenuate abdominal aortic aneurysm in mice. *Cardiovasc Drugs Ther*. 2025;39:239-257. https://doi.org/10.1007/s10557-023-07518-0.
11 Li CW, Cui CB. Application of several physicochemical techniques in natural products to elucidate stereochemistry. *J Int Pharm Res*. 2015;42(6):811-828. https://doi.org/10.13220/j.cnki.jipr.2015.06.016.
12 Politi M, De Tommasi N, Pescitelli G, et al. Structure and absolute configuration of new diterpenes from *Lavandula multifida*. *J Nat Prod*. 2002;65(11):1742-1745. https://doi.org/10.1021/np020260p.
13 Enzell CR, Thomas BR. The chemistry of the order Araucariales. III. Structure and configuration of araucarolone and some related compounds from *Agathis australis*. *Acta Chem Scand*. 1965;19(8):1875-1896.
14 Fujita N, Yoshimoto T and Samejima M. Components of extracts from *Agathis* wood. *Mokuzai Gakkaishi*. 1984;30(3):264-268.
15 Cambie RC, Coddington JM, Stone MJ, et al. Diterpenoids of the wood of *Agathis vitiensis*. *Phytochemistry*. 1989;28(6):1675-1679. https://doi.org/10.1016/S0031-9422(00)97823-3.
16 Heckler K, Kroll J. Zebrafish as a model for the study of microvascular complications of diabetes and their mechanisms. *Int J Mol Sci*. 2017;18(9):2002. https://doi.org/10.3390/ijms18092002.
17 Jia JX, Kang Q, Liu SZ, et al. Artemether and aspterric acid induce pancreatic alpha cells to transdifferentiate into beta cells in zebrafish. *Br J Pharmacol*. 2022;179(9):1962-1977. https://doi.org/10.1111/bph.15769.
18 Li M, Maddison LA, Page-McCaw P, et al. Overnutrition induces β-cell differentiation through prolonged activation of β-cells in zebrafish larvae. *Am J Physiol Endocrinol Metab*. 2014;306(7):E799-807. https://doi.org/10.1152/ajpendo.00686.2013.
19 Lee J, Jung DW, Kim WH, et al. Development of a highly visual, simple, and rapid test for the discovery of novel insulin mimetics in living vertebrates. *ACS Chem Biol*. 2013;8(8):1803-1814. https://doi.org/10.1021/cb4000162.
20 Dalgin GK, Ward AB, Hao LT, et al. Zebrafish mnx1 controls cell fate choice in the developing endocrine pancreas. *Dev Biol*. 2011;356(1):189-189. https://doi.org/10.1242/dev.067736.
21 Bouldin CM, Kimelman D. Dual fucci: a new transgenic line for studying the cell cycle from embryos to adults. *Zebrafish*. 2014;11(2):182-183. https://doi.org/10.1089/zeb.2014.0986.